ELSEVIER

Structural investigations of pyrogenic silica–epoxy composites: Combining small-angle neutron scattering and transmission electron microscopy

Elodie Bugnicourt [a], Jocelyne Galy [a,*], Jean-François Gérard [a], François Boué [b], Herbert Barthel [c]

[a] *Laboratoire des Matériaux Macromoléculaires/IMP, UMR CNRS 5627, INSA-Lyon,*
Bât Jules Verne, 20 Av. A. Einstein, F-69621 Villeurbanne Cedex, France
[b] *Laboratoire Léon Brillouin, UMR 12 CEA/CNRS, CEA Saclay, F-91191 Gif-sur-Yvette, France*
[c] *Wacker-Chemie AG, D-84489 Burghausen, Germany*

Abstract

Small-angle neutron scattering (SANS) and transmission electron microscopy (TEM) were used to investigate the structure of pyrogenic silica in epoxy-based sub-microcomposites. Pyrogenic silica exhibits a fractal-like structure that can be characterized accurately by SANS. Two series of networks were synthesized. In the first series the specific surface area of pyrogenic silica varied from 50 to 300 m^2/g. In the second series, the silica surface was modified in order to be able to react covalently with the precursors of the epoxy network.
© 2006 Elsevier Ltd. All rights reserved.

Keywords: Epoxy networks; Pyrogenic silica; Small-angle neutron scattering

1. Introduction

For the last few years, sub-micron structured materials have been the object of many scientific and technical studies, due to the large impact on a wide range of properties even at low filler content (mechanical, barrier, thermal properties,…). One of the main challenges in the field of nanofiller-based materials consists in controlling the filler dispersion state, because it is directly related to the expected improvement of the final properties. Therefore special attention must be paid to the characterization of the microstructure at different scales of observation. The aim of this work is to study the structuration of pyrogenic silica (also called fumed silica) in an epoxy matrix. Such materials are being developed in order to achieve a mechanical reinforcement of epoxy networks, which are known to be inherently brittle, for the conventional arrays of applications of epoxy such as coatings, adhesives or composites… Filler addition might also result in the enhancement of additional

properties of epoxy matrices such as thermal and dimensional stability, fire resistance, surface hardness…

The filler used in this work, i.e. pyrogenic silica, presents multi-scale organization. It has been extensively used in order to reinforce silicone rubbers, as well as for rheological modifications of coatings, adhesives, sealants and UPR composites, but only a few studies deal with the use of pyrogenic silica in thermosetting polymers [1–4]. Pyrogenic silica is a finely divided amorphous silicon dioxide produced by high temperature hydrolysis of silicon tetrachloride in an oxygen–hydrogen flame [5–7]. Pyrogenic silica particles can be seen at three scales: first, primary particles of around 5–30 nm in size are formed at high flame temperature; second, these particles are not stable and fuse together to form stable aggregates of around 100–250 nm; third, when leaving the flame the silica aggregates stick together by physico-chemical surface interactions (van der Waals' forces), building up large micrometer-sized agglomerates and finally fluffy flocks. Because of the huge specific surface area (50–400 m^2/g) of these particles, the surface silanol functional groups and the surface siloxane bonds play a major role in the behavior of pyrogenic silica. In the

* Corresponding author. Tel.: +33 4 72 43 83 81; fax: +33 4 72 43 85 27.
E-mail address: jocelyne.galy@insa-lyon.fr (J. Galy).

unmodified state, the silanol groups impart a hydrophilic character to the silica surface.

In this work we employed small-angle neutron scattering (SANS) and transmission electron microscopy (TEM) to study the microstructure of pyrogenic silica-based epoxy composites, as a function of the silica specific surface area (SSA) and as a function of the chemical modification of the silica surface (amino- or epoxy-modified silica). In the latter case, the formation of a covalent bond between the modified silica and the matrix was checked [8].

SANS has been applied widely to the study of microstructure of fractal systems [9–12], and it appears to be one of the most appropriate ways to determine the fractal dimensions. The structural information obtained from SANS is analyzed in light of the images obtained from TEM measurements. Here, the limit of a fractal analysis comes mainly from the real structure, where the fractal-like aggregation is often limited in scale compared to the largest size of finite aggregates. Indeed, we want to characterize here this ''real structure'', and compare it with TEM characterization of the same real structure. The combined SANS and TEM results have provided a useful understanding of the microstructure of silica-based epoxy composites. This appears to be one of the first studies on epoxy-containing silica networks combining the two techniques.

2. Experimental

2.1. Materials

The diepoxy prepolymer used was a DGEBA (diglycidyl ether of bisphenol A, DER 330 from Dow Chemicals). It is liquid at room temperature with a viscosity equal to 10 Pa.s at 25 °C. This makes rather easy the mixing with the fillers. On the contrary, the curing agent, a primary aromatic diamine, MDEA (4,4′-methylene-bis(2,6-diethylaniline) from Lonza) is solid at room temperature, therefore no introduction of silica into this comonomer was possible. Chemical structures of both components are displayed in Table 1. MDEA presents a short and rigid chain so that when combined with DER 330 it forms a network of a high cross-link density which is glassy at room temperature, its glass transition temperature is close to 160 °C [8].

A series of hydrophilic silica, called T, N, S and D, with specific surface area (SSA) ranging from 300 to 50 m^2/g

(measured by BET [13]) were studied (see Table 2). These silica are commercially available from Wacker-Chemie AG. The silica N, exhibiting a specific surface area of 200 m^2/g, was used as reference among unmodified silica for most experiments. Note that when changing the SSA, the particle size distribution is also significantly modified. With decreasing SSA, the primary particle size is increased and the size distribution of the primary particles shows more and more polydispersity. Over 300 m^2/g the pyrogenic silica surface becomes micro-porous; this can affect the behavior of the filled systems. For any SSA, the silanol content on the silica surface is considered constant with a value [14] of 1.8 Si–OH per nm^2. Hence, the overall number of silanol groups able to develop interactions with the epoxy matrix is mostly linked to the silica SSA, at a given silica content.

Two main categories of organo-modifications were used, i.e. amino-modified (noted A, a_{50}, and A_p) and epoxy-modified silica (noted E), as listed in Table 2. Each of these potentially reactive modified silica was grafted starting from hydrophilic silica with a specific surface area of 300 m^2/g, with a controlled grafting content (i.e. partial vs. full substitution of the surface silanols). Afterwards, the grafting was checked thanks to elemental analysis of the carbon content and to titrations of the residual silanols on silica surface.

2.2. Composite processing

A precise modus operandi was set up to de-agglomerate pyrogenic silica into individual aggregates and counteract their reflocculation in the organic medium under the action of colloidal forces. The standard process developed for the preparation of the silica suspensions into liquid media used a high-speed disk (65 mm diameter) dissolver (Turbotest 33/300P from Rayneri). The silica was introduced progressively into the epoxy monomer. First, a mixing speed of about 500 rpm was applied, and then after complete incorporation of the silica, the maximum rate (3300 rpm) was used for 1 h. The obtained silica–epoxy suspension was out-gassed and the curing agent was added. The mixture was heated to a temperature of 90 °C in order to melt MDEA and poured in a mould. The curing cycle was 4 h at 135 °C, followed by a post-cure of 4 h at 190 °C. It allows a complete reaction of amino and epoxy groups. All composites were synthesized in stoichiometric conditions (ratio of amino-hydrogen groups over epoxy
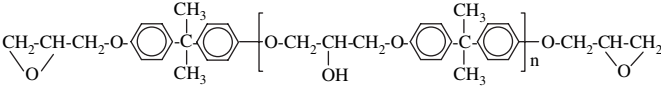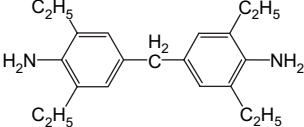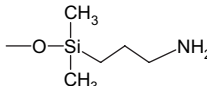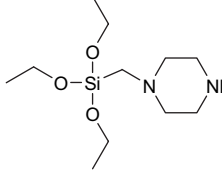
Table 1
Chemical structure of monomers
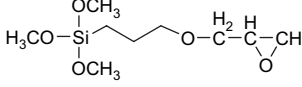
Monomers		
DER 330 (D)	CH$_2$-CH-CH$_2$-O-⟨⟩-C(CH$_3$)(CH$_3$)-⟨⟩-[O-CH$_2$-CH-CH$_2$-O-⟨⟩-C(CH$_3$)(CH$_3$)-⟨⟩]$_n$-O-CH$_2$-CH-CH$_2$ (with OH)	$M_n = 360$ g/mol
MDEA (M)	H$_2$N-⟨C$_2$H$_5$, C$_2$H$_5$⟩-CH$_2$-⟨C$_2$H$_5$, C$_2$H$_5$⟩-NH$_2$	$M = 310.5$ g/mol

Table 2
Characteristics of the different silica used in the study

Silica	Ref. Wacker	SSA (m²/g)	Residual silanols (%)	Surface modification	Modification content (per 100 g of silica)	Structure
T	HDK T30	300	100	None	0	
N	HDK N20	200	100	None	0	
S	HDK S13	125	100	None	0	
D	HDK D05	50	100	None	0	
a_{50}	HKS A/MG 25-1	300	50	Partially amino modified	0.045 mol NH_2	
A	H30RA	300	10—15	Amino-modified	0.09 mol NH_2	CH_3 / $-O-Si(CH_3)_2-...-NH_2$
A_p	SLM 433091/047-1	300	10—15	Amino-modified (piperazino)	0.09 mol NH	(piperazine structure)
E	HKS A/MG 26-1	300	30—40	Epoxy-modified	0.067 mol epoxy	$H_3CO-Si(OCH_3)_2-...-O-CH_2-CH-CH_2$ (epoxide)

groups = 1) with a silica content of 5 wt%. The nomenclature used to label the different samples is DM for the neat epoxy matrix and 5X-DM for the sub-microcomposites filled with 5 wt% of silica, where X is the type of silica used (T, N, S or D, Table 2).

2.3. TEM measurements

TEM examination was completed using a Philips CM120 microscope. The samples were cut, at room temperature, as thin layers (between 60 and 80 nm) using an ultra-microtome with a diamond knife. The thin layers were then placed between copper grids for observation.

2.4. SANS experiments

The SANS experiments were performed with the small-angle scattering diffractometer "PAXE" for most experiments ("PACE" and "PAXY" were used in other cases), at the Laboratoire Léon Brillouin (LLB) at the CEA in Saclay (France). Cold neutrons were used, with three wavelengths lying between 6 and 25 Å, combined with three distances. The resulting total q range covered in three configurations is $[2 \times 10^{-3}, 0.15 \text{ Å}^{-1}]$. The spectra recording required about 20 min for each configuration, a rather short time, owing to the large scattering contrast between the organic medium and silica particles. The data treatment followed standard correction procedures (LLB softwares) to obtain absolute scattering intensity (in cm^{-1}). The following expression was used for these corrections:

$$I(cm^{-1}) = \frac{I_{sample(t,T,C)} - I_{sample\ holder(t,T,C)}}{I_{H_2O(t,T,C)} - I_{empty\ cell(t,T,C)}} \times \frac{d\Sigma}{d\Omega_{water}} \qquad (1)$$

where, $d\Sigma/d\Omega_{water}$ (cm^{-1}) is the scattering cross-section per volume of 1 mm water and I_{sample}, $I_{sample\ holder}$, I_{H_2O} and $I_{empty\ cell}$ are radially averaged recorded spectra corrected by the incident neutron flux, the thickness t, and transmission T, of, respectively, the sample, the sample holder without sample, the water and the water cell without water. C is the volume concentration. For silica powder in dry state or soaked in solvent the sample holder was a glass or a quartz cell, respectively; epoxy—silica composites were solid plates which could be observed directly without sample holder. All composites were about 1 mm thick, with a 20 mm diameter. For each sample, the three spectra obtained for the three configurations are overlapping in the common region between the different q ranges owing to the flux normalisation and wavelength dependent water scattering section corrections. Finally, the incoherent scattering was evaluated from the pure silica and neat epoxy matrix, and subtracted. The incoherent scattering from pure silica was found to be very small. The remaining intensity is mostly the Fourier transform of silica concentration spatial correlations, apart from low-q scattering due to voids, which as we will see can here be neglected.

3. Results and discussion

3.1. Comparison between pristine silica and the same silica in the epoxy-based composite

Firstly, the log—log plots of the neutron scattering intensity I, vs. the neutron scattering vector q, for the pristine silica N and for the epoxy network filled with 5 wt% of the same hydrophilic silica (5N-DM) are shown in Fig. 1. There are some differences between these two patterns at low q: for the former, the increase of scattering intensity is continuous, whereas for the latter, a noteworthy maximum of scattering, is observed at about $3 \times 10^{-3} \text{ Å}^{-1}$. It is known that the shape of $I(q)$ in the low-q range may provide information on the organization of the scattering objects in the medium; more specifically the appearance of a maximum at a wave vector,
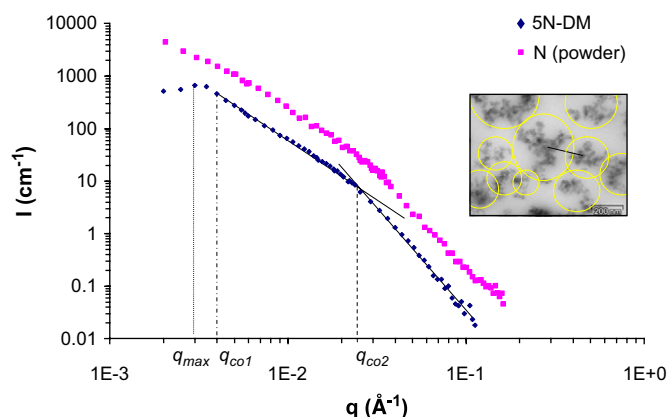
Fig. 1. SANS patterns $I(q)$ for: (◆) cross-linked epoxy-based composite filled with 5 wt% of hydrophilic N silica and (■) pristine N silica (as a powder). On the right: composite morphology.

$$d_{aggr} = \frac{2\pi}{q_{max}} \qquad (2)$$

This value does not correspond, at a silica concentration of 5 wt% in the epoxy composite, to a distance between primary particles, but to a distance of 210 nm between some aggregates. This is in agreement with TEM photos (Figs. 1 and 2). The peak, which is furthermore pronounced in linear scale, cannot be considered as an artifact. We can also remark, on the right hand side of the peak, that the intensity starts to leave the straight line (in log—log plot) and grows faster. In other words, if we were dividing the signal by the form factor of the aggregate (which corresponds to the straight line in this q range), we would observe a structure factor with a pronounced peak. Conversely, for very dilute silica suspension (~ 1 vol%) in deuterated THF no maximum was observed due to the absence of interaction in this case between the aggregates. For the silica powder sample, the peak is also absent because no most probable inter-particular distance exists.

q_{max}, is related to inter-aggregate structure factor, leading to a long distance correlation between the scattering units [15,16]. A preferred spacing between aggregates can be calculated in first approximation according to Bragg's law as:

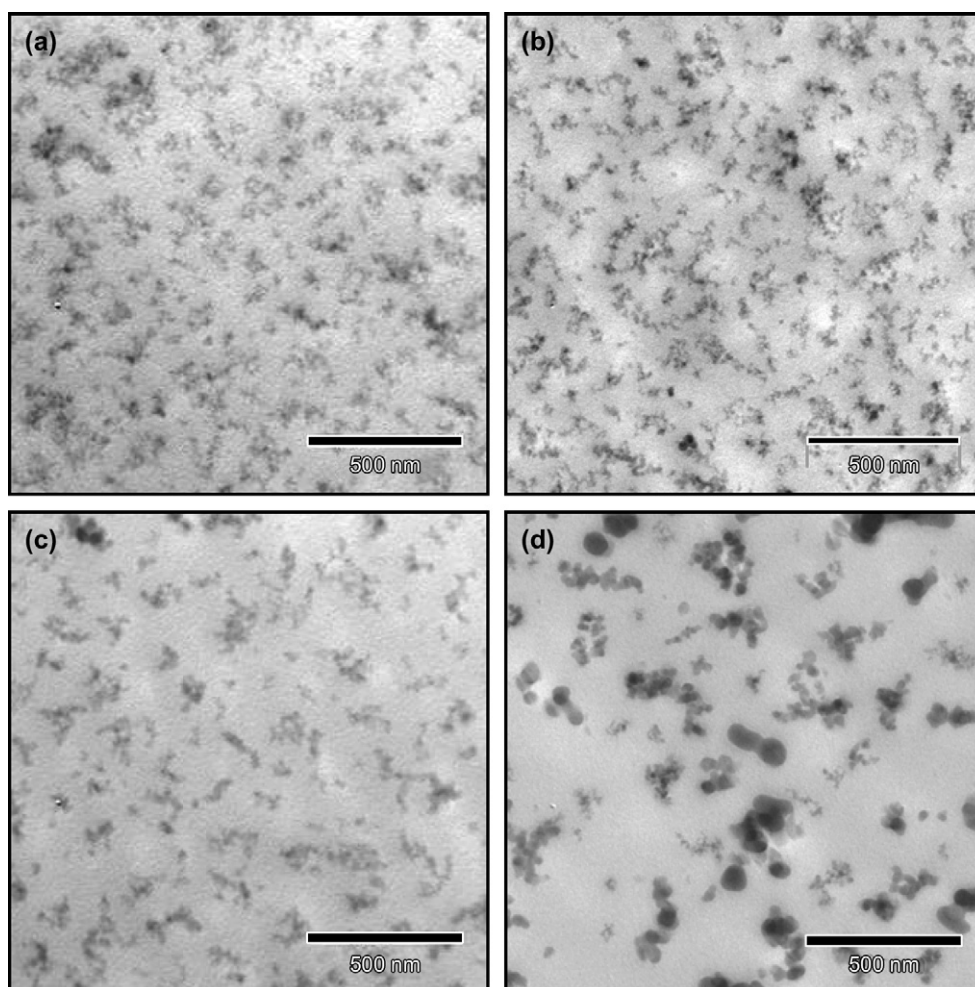The simplest picture for this rather well-defined peak is aggregates of narrowly distributed mass and compact shape

Fig. 2. TEM pictures for epoxy-based composites filled with 5 wt% of hydrophilic silica of different specific surface area: (a) T, 300 m²/g; (b) N, 200 m²/g, (c) S, 125 m²/g; (d) D, 50 m²/g.

separated by a distance d_{aggr} which defines a cube of volume d_{aggr}^3 inside which is located each aggregate. If Φ_{Si} is the silica volume fraction and V_{Si} the volume of the primary particle, we have:

$$\Phi_{Si} = N_{aggr} V_{Si}/d_{aggr}^3 \tag{3}$$

For a primary particle diameter of 10 nm and a volume fraction of 2.27%, this gives an aggregation number $N_{aggr} = 400$. TEM pictures are 2D pictures only but can be considered to be in agreement with this value. However, they suggest a more complicated shape that is linked with the apparent fractal dimension of aggregates, which will be discussed below. Also, we observe sizes often larger than the inter-aggregate distance of 210 nm; in other words, the system is partly interpenetrated. In this case, the privileged distance cannot be directly linked to the concentration as proposed in the equation above.

At larger q, the features of the two plots for the pristine silica and for the filled epoxy network are rather similar, the two curves are essentially parallel. This means that the scattering objects are identical at the corresponding scales. This occurs not only at the primary particle scale, which was expected, but also in the intra-aggregate size range, meaning that their inner organization is also identical. We can characterize this size range by two parameters (all their numerical values can be found in Table 3):

◆ The first one is the slope, α_1, at lower q, of the straight line observed in the log—log plot, which corresponds to a power law $q^{-\alpha_1}$. This characterizes the mass fractal-like distribution of the primary aggregates with an apparent value, $D_m = \alpha_1$.

◆ The second one is the slope α_2, at high q; in this range, since the primary particles are compact, the slope can only be characteristic of the interface between the particles and the matrix. If the latter was sharp, a q^{-4} Porod law would be observed; here, the slope is lower than 4. This is explained by the formula $\alpha_2 = 6 - D_s$, where D_s is the apparent surface fractal dimension of the primary particle; D_s is slightly larger than 2.

The error on the apparent slopes is of the order of ± 0.05 at small q (i.e. apparent mass fractal dimension) and of ± 0.1 at high q (i.e. apparent surface fractal dimension) unless noted in Tables 3—5.

The crossover between these 2 linear regions in log—log plots is located at a q value, q_{co2}, characteristic of the particle size [17],

$$R_{g2} = \frac{1}{q_{co2}} \tag{4}$$

Here R_{g2} is taken as a radius of gyration usually related, for compact spheres, to the sphere radius R by:

$$R^2 = \frac{5}{3}R_g^2 \tag{5}$$

Such interpretations are currently used in the literature [18—20]. The diameter, $\Phi_{pp} = 2R$, obtained for the primary particles (~ 10 nm), given in Table 3, is in the range expected. Its variation with silica specific surface area will be discussed in detail further in the following section.

An additional parameter is the radius of gyration of the aggregates, R_{g1}. If no inter-aggregate correlation size appears, we can assume a Guinier law, $I(q) \sim 1 - q^2 R_g^2/3$, in the low-$q$ regime ($q < 1/R_{g1}$). Then R_{g1} is obtained from the crossover

Table 3
Structural features obtained from the analysis of SANS patterns of the pristine silica N and of the cross-linked epoxy-based composite filled with 5 wt% of hydrophilic N silica

Sample	Shape at low-q	q_{co1} (Å^{-1})	$2R_{g1}$ (nm)	D_m (± 0.05)	q_{co2} (Å^{-1})	Φ_{pp} (nm)	D_s (± 0.1)
Silica N	Continuous increase	−	−	2.28	0.027	9.9	2.3
5N-DM	Max: $d_{aggr} = 210$ nm	0.0040	50	2.23	0.024	10.9	2.2

Table 4
Structural features obtained from the analysis of SANS patterns of the cross-linked epoxy-based composite filled with 5 wt% of hydrophilic silica with different SSA

Sample	SSA (m^2/g)	Shape at low-q	q_{co1} (Å^{-1})	$2R_{g1}$ (nm)	D_m	q_{co2} (Å^{-1})	Φ_{pp} (nm)	D_s (± 0.1)
5T-DM	300	Plateau	0.0040	50	2.45 ± 0.05	0.027	9.5	2.8
5N-DM	200	Max: $d_{aggr} = 210$ nm	0.0040	50	2.23 ± 0.05	0.024	10.9	2.2
5S-DM	125	Inflexion	0.0031	64	2.43 ± 0.1	0.017	14.8	2.36
5D-DM	50	Inflexion	0.0031	64	2.3—2.6	0.008	32.2	2.2

Table 5
Structural features obtained from the analysis of SANS patterns of the cross-linked epoxy-based composite filled with 5 wt% of different modified silica

Sample	Shape at low-q	q_{co1} (Å^{-1})	$2R_{g1}$ (nm)	D_m (± 0.05)	q_{co2} (Å^{-1})	Φ_{pp} (nm)	D_s (± 0.1)
5T-DM	Plateau	0.0040	50	2.45	0.027	9.5	2.8
5a$_{50}$-DM	Non-accessible	0.0023	86	2.01	0.026	9.9	2.5
5A-DM	Intersection plateau	0.0025	80	2.01	0.022	11.9	2.75
5A$_p$-DM	Non-accessible	0.0035	57	2.09	0.022	11.5	2.4
5E-DM	Non-accessible	0.0031	65	2.14 ± 0.02	0.024	10.7	2.8

with the low-q regime, q_{co1}, corresponding roughly to the inflexion of the curve:

$$R_{g1} = \frac{1}{q_{co1}} \qquad (6)$$

In our systems, where the apparent fractal dimensions are not too different, the proportionality factor between R_{g1} and the geometric size (radius R) should not change. R_{g1} is known to be largely lower than R for "open" fractal-like objects such as pyrogenic silica aggregates. The radius of gyration of the aggregates for the epoxy nanocomposite considered here, found equal to 25 nm from SANS pattern, is rather consistent with the structure observed. Hence the models used are validated for the epoxy nanocomposite considered here.

3.2. Effect of the specific surface area

The TEM pictures and the SANS patterns of the composites filled with hydrophilic silica of various specific surface area are reported in Figs. 2 and 3, respectively. For epoxy networks filled with hydrophilic silica, a homogeneous, optimal dispersion state was obtained whatever the specific surface area (from 50 up to 300 m^2/g). This morphology was attributed to the very good interactions developed between the polar epoxy matrix and silica surface silanols which favor particle–polymer interactions rather than particle–particle interactions. As already mentioned, and as it is clear from these images, the primary particle size and size distribution are larger for the lowest specific surface area (50 m^2/g, Fig. 2d).

Let us now look at SANS plots (I vs. q, Fig. 3), and at the parameters extracted from the intensity, reported in Table 4. Here also notable and consistent differences are observed. In the large q region, the lower the specific surface area (i.e.
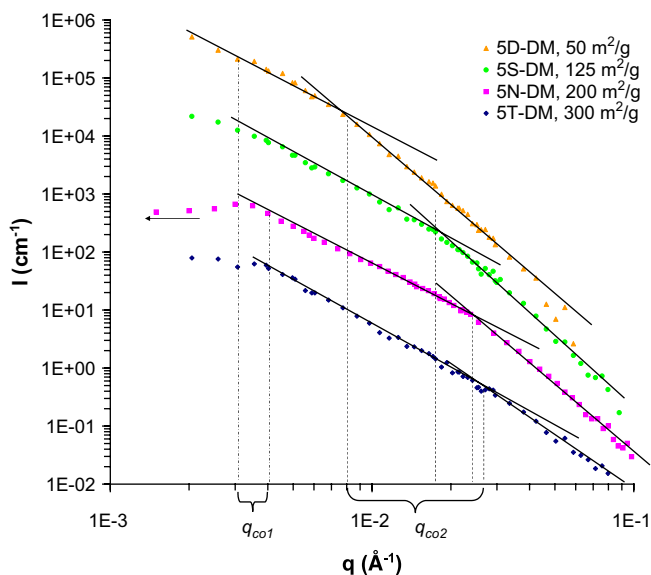

Fig. 3. SANS patterns $I(q)$ for epoxy-based composites filled with 5 wt% of hydrophilic silica of different surface specific area: (◆) T, 300 m^2/g; (■) N, 200 m^2/g; (●) S, 125 m^2/g; (▲) D, 50 m^2/g (for more clarity curves have been shifted on the Y-axis of 2 decades for 5D-DM, 1 decade for 5S-DM and −1 decade for 5T-DM as compared to 5N-DM).

network 5D-DM), the lower the intensity values (Fig. 3). Moreover the slope is lower for high SSA. Since the generalized "Porod" law is $q^{-(6-D_s)}$, this means that higher SSA corresponds also to a higher apparent surface fractal dimension. This observation describes a rougher surface as the specific surface area increases. This might be related to the microporosities for silica of SSA equal or above 300 m^2/g. In contrast, at the lowest specific surface area (50 m^2/g), the silica exhibits a simple smooth surface characterized by a surface fractal dimension close to 2, i.e. by a q^{-4} "real" Porod law.

The crossover between "Porod" and "mass fractal" regions, q_{co2}, characterizing the size of the primary particles, varies gradually as a function of silica specific surface area. The primary particle size is found to increase from 9.5 to 32.2 nm as the SSA of silica decreases from 300 to 50 m^2/g. This result is in agreement with the TEM observation.

At lower q, on the left part of the $I(q)$ plot, we have more detailed information on the organization and size of aggregates averaged over the whole sample. For the higher specific surface area (T), the behavior is the one already described for silica N: when decreasing q, a constant slope is first observed, which has been attributed to an apparent mass fractal dimension and is similar for T and N. At lower q, a plateau and a maximum are observed, signaling a privileged distance between aggregates of well-defined size. For the lower specific surface area (D and S), i.e. for larger elementary particles, the slope is more difficult to evaluate, especially for sample 5D-DM. The intensity increases, while no maximum is observed. This difference might be either due to the fact that it is not visible in the q range analyzed, or because it is more progressive owing to the higher size polydispersity and to larger particles.

In summary, although the same apparent type of fine morphology was shown by TEM for epoxy-based systems filled with hydrophilic silica of any specific surface area, SANS provided a further insight into their difference.

3.3. Comparisons between the diameters of primary particles obtained by SANS and other techniques

Sizes and measurement techniques of the primary and secondary structures in pyrogenic silica are still a matter of discussion [7,21]. Indeed, the values worked out are largely different depending on the technique used. Diameters of the primary particles measured by SANS in situ in the epoxy-based composites are plotted in Fig. 4 against the results of the theoretical diameter calculated from BET measurements. BET theory is a well-known rule for the physical adsorption of gas molecules on a solid surface [13] and the BET method is now widely used in surface science for the calculation of surface area of solids and powders. The diameter, d_{BET}, found according to BET measurements is obtained by:

$$d_{BET} = \frac{6}{\rho SSA_{BET}} \qquad (7)$$

where ρ is the density of amorphous silica (2.2 g/cm^3). It turns out that SANS results correlated linearly with those of BET,
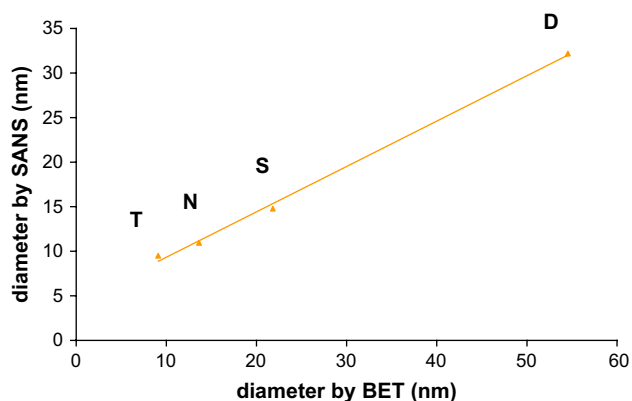
Fig. 4. Comparison of the diameters of primary particles of the different silica, obtained by SANS and BET measurements.

while values from SANS are systematically lower. The offset when extrapolating the curve to $d_{BET} = 0$ was rather small (expectedly nil). The difference increases as the diameter found by BET increases; this might be not only due to the sensitivity of the different methods to the polydispersity of the primary particles forming the aggregates but also due to the fact that the primary particles are fused together. Therefore part of their

surface is not accessible to the gas adsorption in the BET method, this phenomenon is enhanced for larger primary particles.

3.4. Effect of the silica surface treatment

The micrographs obtained by TEM on epoxy networks filled with 5 wt% of different amino- and epoxy-modified silica, of the same specific surface area (300 m²/g before surface modification) are shown in Fig. 5. For fully amino-modified silica, A, (Fig. 5a) the main part of the aggregates is well dispersed, but some large (∼5 μm) and relatively compact agglomerates remain. For partially amino-modified silica (Fig. 5b), with a substitution of only 50% of the initial silanol groups using the same amino-silane, the dispersion obtained is almost uniform, only a few small regions of low compactness (<1 μm) can be noticed. Thus, if we compare with unmodified silica which is well dispersed, we conclude that the dispersion state turns out to be favored by the silanols present at the surface. Contrary to the case of fully amino-modified silica, A, a good dispersion state can be reached with fully piperazino-modified silica, A_p as seen on Fig. 5c, with no notable agglomerates larger than the micron scale. Finally, for epoxy-modified
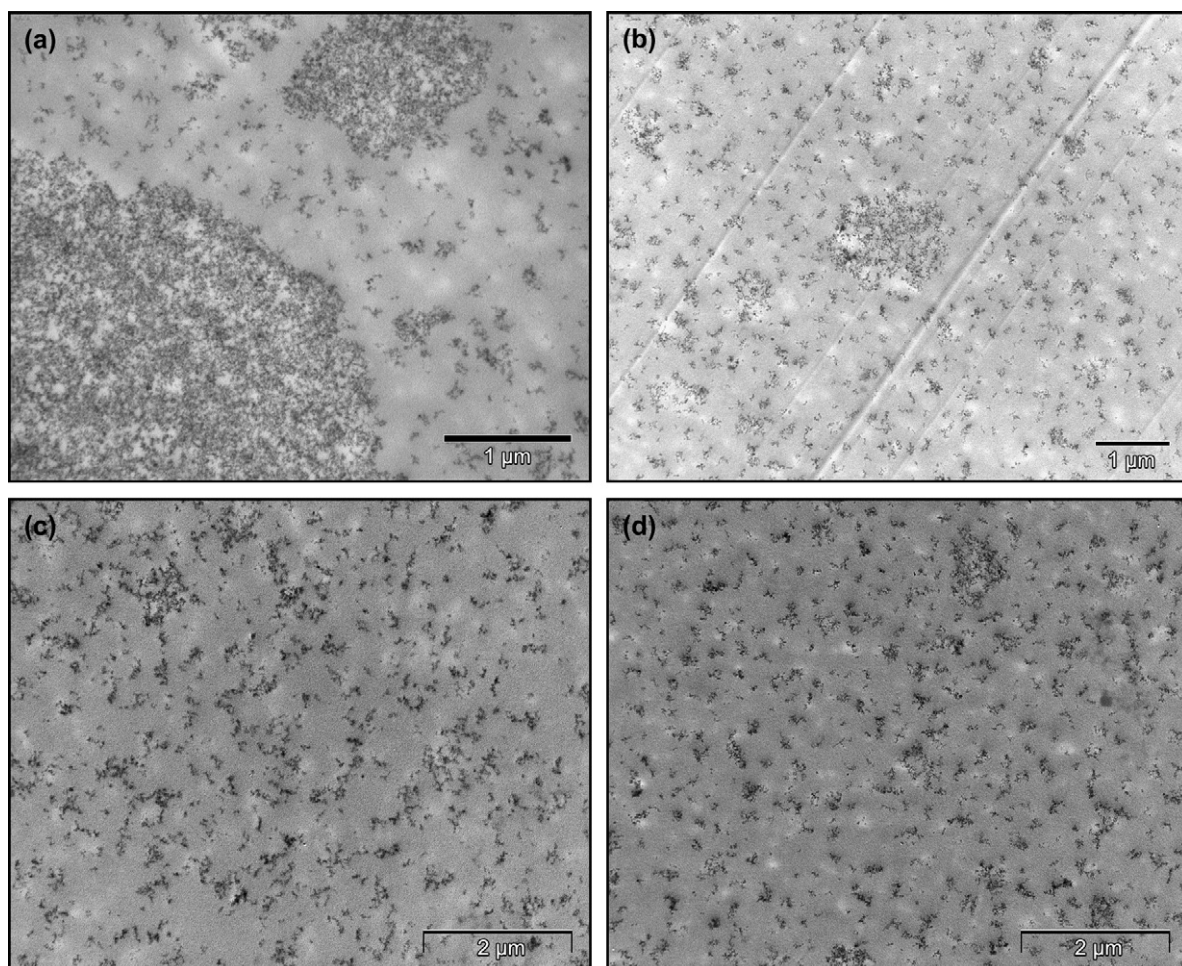

Fig. 5. TEM pictures for epoxy-based composites filled with 5 wt% of modified silica: (a) fully amino-modified A; (b) 50% amino-modified a_{50}; (c) piperazino-modified A_p; (d) epoxy-modified E.

silica, the dispersion obtained is also good with no compact silica region larger than the micron scale.

We now turn towards the SANS signature of these surface-modified silica. The SANS patterns of a reference cross-linked epoxy system filled with the untreated N silica (5N-DM), taken as a standard, are compared with that of a system filled with a fully amino-modified A silica (5A-DM) in Fig. 6. No maximum is observed for amino-modified silica A-based epoxy composite, at variance with hydrophilic silica N-based epoxy composite.

At this stage, let us discuss the shape of SANS curves in relation with the coexistence of silica in well-dispersed regions and in more or less compact agglomerates. The agglomerates observed in TEM pictures are too large to be detected as individual scattering objects in the q-window analyzed (Bragg distances limited up to approximately 300 nm). Their contribution to the scattering comes from their inner structure or their surface; it depends on the compactness of the agglomerates:

(i) if the agglomerates are fully compact, i.e. there is no epoxy matrix between the aggregates forming the agglomerates, their scattering is of the Porod type, $q^{-\alpha \sim 4}$. Whereas it is very large in a low-q region $qR_{aggr} \sim 1$, not available here ($< 10^{-3}$ Å^{-1}), it has decreased a lot when reaching the available q ranges. In other words, since in this range the scattering is proportional to the specific area of the agglomerates, it is very low for these very large agglomerates (S/V varies inversely to the size).

(ii) if, on the contrary, the agglomerates are not fully compact (which is more likely to be true after TEM images) some scattering can come from the inside of the agglomerates, which makes them "visible" by neutron
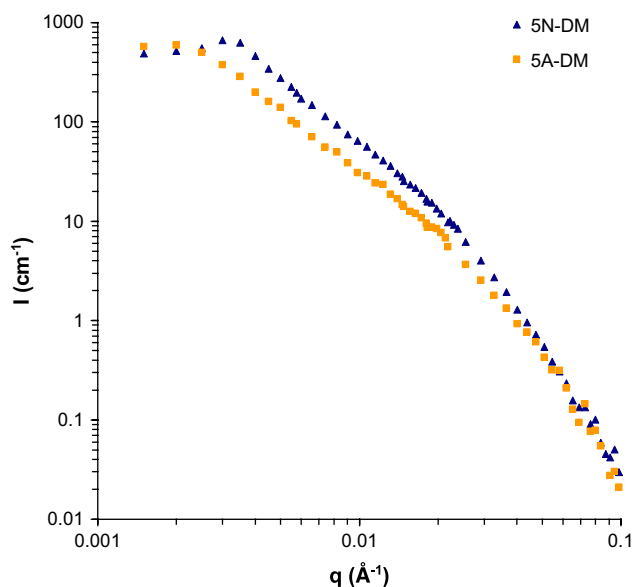
scattering in our available q range. At even larger q, the scattering comes from the inside of the aggregates; it cannot be distinguished from the one of well-dispersed aggregates. Since the overall quantity of particles is constant, the intensity level is not expected to change markedly at large q. We observe this in Fig. 6, but only at large $q > 5 \times 10^{-2}$ Å^{-1}. At intermediate q, i.e. 4×10^{-3} Å$^{-1} < q < 2 \times 10^{-2}$ Å^{-1}, the A silica signal appears shifted by a factor ~ 2 lower than the N silica signal. This means that a fraction of about 50% of the A silica signal seems to be lacking compared to N silica. This fraction can be contained in the large compact agglomerates, the remaining being in the dispersed phase as aggregates. At lower q, the onset of a maximum produces a slight upturn in the N signal, while the A signal keeps the same slope. The A signal plateaus at $q \sim 2 \times 10^{-3}$ Å^{-1}, signaling that the dispersed phase is made of small aggregates, with no inter-correlation.

In summary this comparison between A and N leads to the conclusion that we can still have much information, at least on the dispersed phase of aggregates.

Fig. 7 presents a comparison at a constant SSA of 300 m^2/g of the SANS patterns of the different amino- and epoxy-modified silica networks studied as compared to the unmodified hydrophilic T silica-based network. The different parameters deduced from these patterns are reported in Table 5. The crossover between "mass fractal" and "Porod" q ranges is roughly the same for all silica ($q_{co2} \sim 0.023$ Å^{-1}) whatever the surface treatment, which is consistent with the fact that the size of the primary particle is not changed by the chemical modification.

The only silica for which a plateau is reached at low q is the hydrophilic T silica. For surface-modified silica, a downturn is observed at low q, which generally slightly shifts towards lower q values as the presence of denser zones seen on TEM frames increases. The radius of gyration, R_{g1}, can be worked out in such low q and can be attributed to the indivisible aggregates/agglomerates. In these systems, R_{g1} is consistently greater for modified silica than for hydrophilic silica. One could also imagine that the signals tend towards some maximum, located at even lower q; the abscissa of such maximum would then decrease, either because the aggregates in the dispersed phase are larger, or because they keep the same size but their concentration is weaker.

At intermediate q, the increasing presence of dense silica regions in the network (case of 5A-DM network) seems to lead to a lowering of the intensity. This decrease of scattering level at a given q might be related to the decrease of the concentration of well-dispersed silica aggregates in the matrix, as just discussed above. Such q dependent decrease could explain the apparent decrease of the slope in the "mass fractal" region. In reality, the apparent mass fractal dimension D_m should not vary after grafting because of the stiffness of the pristine aggregates. The effects just described are strongest for the amino-modified silica. They are reduced for partially amino-modified silica. Among modified silica, best dispersions are achieved
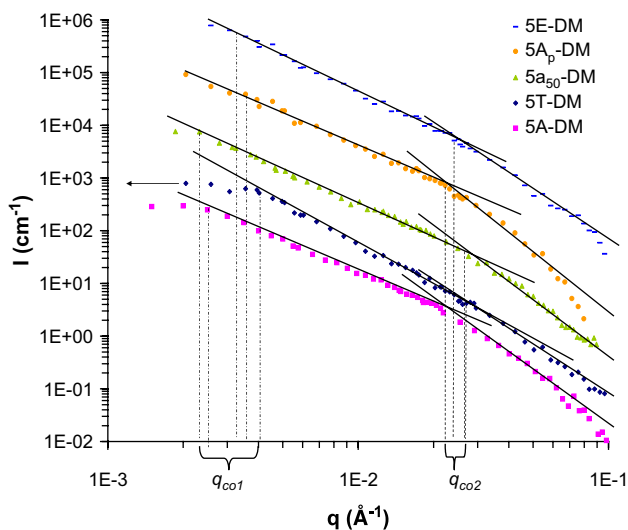

Fig. 6. SANS patterns $I(q)$ for epoxy-based composites filled with 5 wt% of (▲) hydrophilic silica N, 200 m^2/g or (■) amino-modified silica A, 300 m^2/g.

Fig. 7. SANS patterns $I(q)$ for epoxy-based composites filled with 5 wt% of different types of surface-modified silica, with the same SSA of 300 m^2/g before treatment: (−) E, epoxy-modified silica; (●) A$_p$, piperazino-modified silica; (▲) a$_{50}$, partially amino-modified silica; (◆) T, hydrophilic silica of SSA 300 m^2/g; (■) A, fully amino-modified silica (for more clarity curves have been shifted on the Y-axis of 3 decades for 5E-DM, 2 decades for 5Ap-DM, 1 decade for 5a$_{50}$-DM and −0.5 decade for 5A-DM as compared to 5T-DM).

for piperazino-modified, A$_p$, and epoxy-modified silica, E. But all intensities and apparent slopes are always lower for every organo-modified silica than that for hydrophilic silica.

4. Conclusions

Two series of pyrogenic silica-filled epoxy composites were synthesized and characterized using TEM and SANS. In the first series, the specific surface area of pyrogenic silica was varied, and as a consequence the number of surface silanol groups available to interact with the epoxy matrix also varied. In the second series, the silica surface was modified by grafting some amino or epoxy groups, able to create covalent bonds with the matrix. Such new potentialities could have a drawback concerning the dispersion in the matrix. Indeed, dispersion morphologies were shown to depend markedly on silica surface chemistry: except in the case of amino-modified silica where large agglomerates appear to coexist with well-dispersed aggregates, all the other silica are in majority very well dispersed in the epoxy network as demonstrated by TEM. This shows that a fine tuning of the silica surface chemistry is needed to still control dispersion.

SANS appeared as a valuable technique for the investigation of the micro- and nanostructure of such composite materials based on a thermosetting epoxy matrix. However, it is not commonly used in the field of thermosetting polymers. SANS measurements confirmed and enriched the morphological information that has been obtained via TEM observation. This study gave access to information related to the silica structure because the signal of the polymer is much lower than that of the silica; furthermore the aggregates being rather stiff, their

structure is not significantly changed in the composite materials compared to the silica as a powder, except in the extreme left part of the patterns. In this region, which gives access to the larger scale organization of the aggregates, differences exist between the different composite formulations.

The study of the influence of the specific surface area proved interesting. Even though silica was often studied via SANS, to our knowledge, no systematic SANS study as a function of the specific surface area in an epoxy thermoset matrix had been achieved so far and related to SSA results.

In contrast, for surface-modified silica, the influence of the presence of denser silica regions was more difficult to evaluate and it is believed that the use of Ultra SANS would be more fruitful in the future for the study of these systems in order to detect straightforwardly the agglomerates and distinguish the scattering contribution of each type of species in the sample. However, SANS has provided us here a precise description, with a large statistical average (compared to TEM), of at least the dispersed phase.

To end this paper, we return to the aim of such sub-micrometer composites which is to obtain materials with improved performances. The obtained mechanical properties will be the object of forthcoming papers. We will see that the fine structural investigation achieved here depending on silica SSA and surface modification, can help to understand the influence of the different types of morphologies of silica–epoxy composites on their properties.

Acknowledgements

References

[1] Preghenella M, Pegoretti A, Migliaresi C. Polymer 2005;46:12065–72.
[2] Zheng Y, Zheng Y, Ning R. Materials Letters 2003;57:2940–4.
[3] Anderson DP, Benson Tolle T. Polymeric Materials Science and Engineering 2000;220–1.
[4] Fiedler B, Wichmann MHG, Prado LAS, Gojny FH, Schulte K. Interfaces and interphases in multicomponent materials, September 12–14, Lyon, France; 2005.
[5] Wacker-Chemie AG, Silicone Division, Technical brochure, Products and applications – Wacker HDK® Pyrogenic silica. Munich, Germany; 2001. 8 p.
[6] Wacker-Chemie AG Web Site [on line]. Munich, Germany: Wacker-Chemie GmbH, available on: http://www.wacker.com.
[7] Barthel H. Colloids and Surfaces 1995;101:217–26.
[8] Bugnicourt E. Ph.D. thesis, 2005-ISAL-00113.
[9] Teixeira J. Journal of Applied Crystallography 1988;21:781–5.
[10] Cousin F, Oberdisse J, Boué F. Neutron News 2003;14(3):31–4.
[11] Beaucage G, Ulibarri TA, Black EP, Schaefer DW. Hybrid organic–inorganic composites. ACS; 1995. p. 97–111.
[12] El Shafei GMS. In: Papirer E, editor. Adsorption on silica surfaces. NY: Marcel Dekker; 2000.
[13] Brunauer S, Emmett PH, Teller E. Journal of American Chemical Society 1938;60:309.

[14] Barthel H, Heinemann M, Stintz M, Wessely B. Chemical Engineering and Technology 1998;21:745—52.

[15] Cotton JP, Nallet F. Diffusion de neutrons aux petits angles, Ecole thématique de la société française de neutronique. Les Ulis: EDP Sciences; 1999. 194 p.

[16] Qiu D, Dreiss CA, Cosgrove T. Langmuir 2005;21(22):9964—9.

[17] Boyard N. Ph.D. thesis, Physico-chimie des Matériaux, Université d'Orléans; 2003. 286 p.

[18] Espinat D. Revue de l'institut français du pétrole 1990;45(6): 3—44.

[19] Hajji P, David L, Gérard JF. Journal of Polymer Science B 1999;37: 3172—87.

[20] El Harrak A, Carrot G, Oberdisse J, Eychenne-Baron C, Boué F. Macromolecules 2004;37:6376—84.

[21] Babick F, Ripperger S. Particle and Particle Systems Characterization 2002;19:176—85.